Design, analysis and experimental testing of BPSK homodyne receivers based on subcarrier optical phase-locked loop

Design, Analysis and Experimental Testing of BPSK Homodyne Receivers Based on Subcarrier Optical Phase-Locked Loop

Stefano Camatel, *Member, IEEE*, and Valter Ferrero, *Member, IEEE*

***Abstract*—The analysis of a subcarrier optical phase-locked loop (SC-OPLL) is carried out in order to optimize phase-locking performance. A new parameters optimization procedure, useful for OPLL design, is demonstrated theoretically and experimentally. An SC-OPLL based on this procedure has been realized, so a pilot carrier SC-OPLL and a nonlinear SC-OPLL optical receiver have been experimentally constructed and tested. An 8B/10B line coding is employed for pilot carrier SC-OPLL receiver in order to improve performance and a new architecture of decision-driven PLL is experimentally demonstrated.**

***Index Terms*—Homodyne detection, optical phase-locked loops (OPLL), phase noise, phase-shift keying (PSK).**

I. Introduction

HOMODYNE receivers for optical phase-shift keying (PSK) communication systems were investigated in the past and are still attractive because of their several advantages: higher spectral efficiency and longest transmission distance for both free-space and optical fiber communication systems.

A possible implementation of a coherent receiver is based on optical phase-locked loops (OPLL) where a local oscillator (LO) locks the phase of the incoming signal. Many LO were proposed in the past: at the beginning, OPLLs employed, as LO, a HeNe external cavity laser, CO2, or Nd:YAG lasers, with tuning operations performed by a piezoelectric mechanical transducer [1]. Due to the limited piezoelectric transducer time response, they presented some problems to lock the RX signal frequency. Some experiments have been performed by external cavity semiconductor lasers (ECL) with a $\mathrm{LiNbO_3}$ phase modulator inside the cavity, in this case, frequency modulation was obtained by directly driving the two-electrode chip [2]. The use of an acousto-optic modulator was also proposed in order to tune the frequency of a CW HeNe gas laser [3]. Multi-electrode DFB lasers were also used [4]; they respond to a frequency modulation with a reduced phase rotation. Several OPLL designs are known; the most common are balanced OPLLs [3], [5]–[7] and Costas or decision-driven OPLLs [4], [8]–[11]. This paper regards the design of binary PSK (BPSK) homodyne receivers including a subcarrier optical PLL (SC-OPLL) [12], [13], which operates thanks to a particular implementation of the LO based on subcarrier modulation. In fact, the optical voltage controlled oscillator (OVCO) is obtained by externally modulating an LO laser and it is tuned by controlling an electrical VCO. This way, the OVCO characteristics are determined by the electrical VCO.

In this paper, we theoretically analyze the SC-OPLL and evaluate the effect of loop filter configurations on phase locking performance. We propose a new OPLL performance optimization method and demonstrate its efficiency by means of OPLL experimental characterization. We implemented two 2.5 Gb/s homodyne optical receivers based on SC-OPLL: a pilot carrier scheme and a decision-driven scheme. We show that the pilot carrier receiver performance is pattern-dependent, so an 8B/10B line coding is proposed and demonstrated as possible solution. In order to avoid pattern- dependent performance, a decision-driven SC-OPLL is tested as well, giving so the chance to compare the performance of the two implemented receiver configurations.

The remainder of this paper is organized as follows. A general description of the SC-OPLL is given in Section II as well as a theoretical analysis and an experimental characterization. In Section III, two PSK transmission experiments were carried out and their measurement results are compared. Finally, in Section IV the conclusion

II. SC-OPLL

A. SC-OPLL Architecture

The SC-OPLL was presented the first time in [12] and its architecture is shown in Fig. 1(a). The external cavity laser *A* generates the optical signal to be locked by the local oscillator (LO). The polarization controller matches the polarization state of received RX and LO signals, which are then combined by a 3-dB coupler and sent to an amplified photo-diode. The proposed architecture employed a single photo-diode, but a couple of balanced photo-diodes could be used instead [5], [14], [15]. Although the use of balanced photo-detectors would guarantee better performances (approximately 3 dB better in terms of receiver sensitivity), the experimental results obtained with the proposed architecture are enough for a proof of the SC-OPLL proper operation. The electrical signal at the photo-detector output is then processed by an active filter, realized by an SMD board, which includes a compensating dc voltage circuit. The bias voltage V_b is set equal to the signal dc component at the

Manuscript received June 9, 2007; revised November 7, 2007. This work was supported in part by Italian Ministry of University and Research (MIUR), by the STORiCo Project PRIN 2005, and by the EU FP6 Network of Excellence e-Photon/ONe, WP5, and WP10.

S. Camatel is with PhotonLab, Istituto Superiore Mario Boella, 10138 Torino, Italy (e-mail: camatel@ismb.it).

V. Ferrero is with Dipartimento di Elettronica, Politecnico di Torino, 10129 Torino, Italy.

Digital Object Identifier 10.1109/JLT.2007.916504

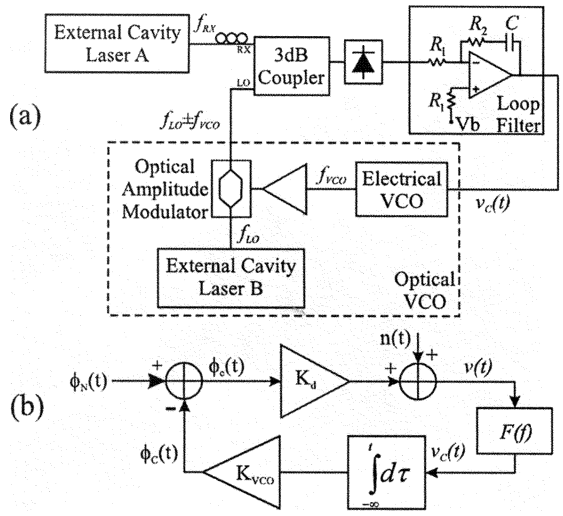

Fig. 1. Schematic diagram of (a) the SC-OPLL and (b) its equivalent linear model.

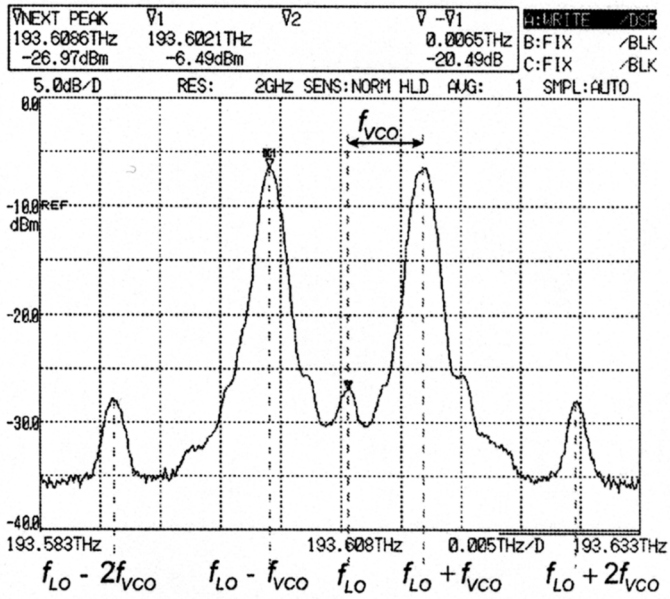

Fig. 2. Optical power spectrum measured at the output of the optical VCO.

photo-diode output. Electrical signal at the loop filter output is finally sent to the OVCO input.

The loop filter parameters setting is fundamental for SC-OPLL proper working, so the design of the loop filter parameters $\tau_1 = R_1C$ and $\tau_2 = R_2C$ is deeply described in the following subsection.

OVCO is the key element of the SC-OPLL and it is based on a commercial CW external cavity tunable laser at frequency $f_{\rm LO}$. The CW laser is externally amplitude modulated by the signal coming from an electrical VCO at frequency $f_{\rm VCO}$. By biasing the external Mach–Zehnder (MZ) amplitude modulator at a null of its transfer function, a sinusoidal carrier-suppressed modulation is obtained. The resulting spectrum at the output of the OVCO is shown in Fig. 2. Two main SCs at frequency $f_{\rm LO} \pm f_{\rm VCO}$ are generated, with spurious optical tones at $f_{\rm LO}$ and $f_{\rm LO} \pm 2 \cdot f_{\rm VCO}$. Using one of the two main SCs, for example the one at $f_{\rm LO} + f_{\rm VCO}$, we are able to tune an optical frequency by simply changing the voltage applied to the electrical VCO, thus implementing an OVCO. The OVCO tuning performance is given by the electrical VCO speed and stability.

Furthermore, coarse (and slow) optical frequency tuning may be obtained by changing the external cavity CW frequency, while fine (and fast) frequency tuning may be obtained varying the VCO control voltage $v_c(t)$.

For OPLL operations, a second-order PLL control circuit sets the $f_{\rm LO} + f_{\rm VCO}$ line to lock the received signal carrier at frequency $f_{\rm RX}$. When the OPLL is locked to $f_{\rm LO} + f_{\rm VCO} = f_{\rm RX}$, the system tracks the incoming optical signal frequency and phase. At the photo-diode output, the received signal is shifted to baseband, so optical homodyne receiver operations are obtained. In principle, due to beating with the other SCs and spurious lines at the OVCO output, the incoming signal spurious copies also appear around frequencies $f_{\rm VCO}$ and $2 \cdot f_{\rm VCO}$, but they are filtered out by the RX electrical filter setting $f_{\rm VCO}$ which is much higher than the RX electrical bandwidth. In the experiments presented in the following sections, the photo-diode has responsivity equal to 800 V/W and bandwidth of 1.8 GHz, while the optical VCO includes a 10 GHz $LiNbO_3$ MZ modulator and a 6-GHz electrical VCO. The proposed configuration makes spurious contributions at the photo-diode output negligible. In order to use this receiver for WDM applications, it is necessary to filter out the mentioned LO spurious spectral component, especially for 40 Gb/s systems. This can be performed by using high frequency VCOs (20–40 GHz) and optical filtering.

A theoretical analysis of the proposed architecture is in the following.

B. Theoretical Analysis

As described in [16] an equivalent linear model [see Fig. 1(b)] can be obtained. In the following, a short theoretical description is presented, which is based on the notations and the fundamental formulae introduced in [17]. Here, we assume a second-order PLL with an active filter. The configuration we analyze is shown in Fig. 1(a), where the source laser is not modulated and the received signal is a CW. The OPLL performance is then estimated through the phase-error variance

$$\sigma^2_{\rm TOT} = \int_{-\infty}^{\infty} S_{\rm PN}(f)|1-H(f)|^2 df + \int_{-\infty}^{\infty} S_{\rm AN}(f)|H(f)|^2 df \quad (1)$$

where $S_{\rm PN}(f)$ is the double-sided phase-noise power spectral density (PSD), originating from source and local oscillator lasers, $S_{\rm AN}(f)$ is the double-sided amplitude noise PSD originating from electrical amplifiers and photo-diode shot-noise. $H(f)$ is the OPLL closed-loop transfer function and it is given by

$$H(f) = \frac{\Phi_C(f)}{\Phi_N(f)} = \frac{\frac{K_{\rm DC}F(f)e^{-j2\pi f\tau}}{(j2\pi f)}}{1+\left[\frac{K_{\rm DC}F(f)e^{-j2\pi f\tau}}{(j2\pi f)}\right]} \quad (2)$$

where $K_{\rm DC} = K_d K_{\rm VCO}$ is the open-loop OPLL total gain (see [17]) and τ is the loop propagation delay. K_d and $K_{\rm VCO}$ are

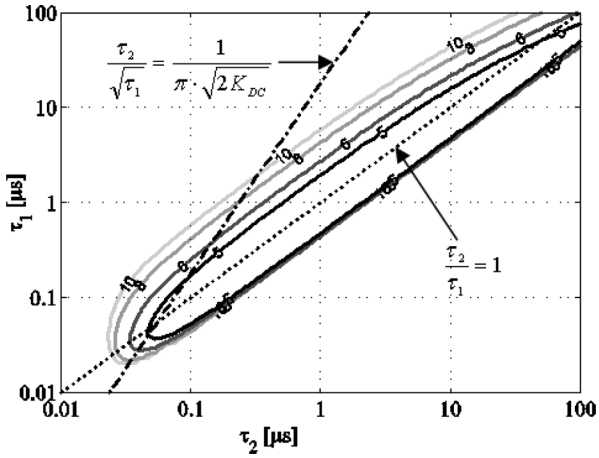

Fig. 3. Level curves of the phase error standard deviation σ_{TOT} (expressed in degrees) function of $\tau 1$ and $\tau 2$ obtained by a theoretical analysis.

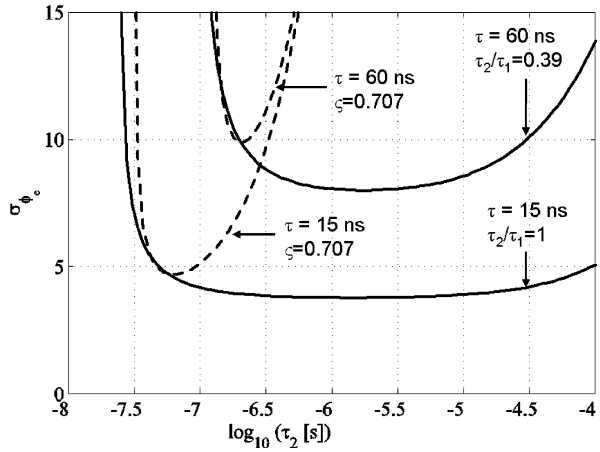

Fig. 4. Computed phase-error standard deviation versus τ_2 for the two conditions damping factor $\zeta = 1/\sqrt{2}$ and $\tau 2/\tau 1 =$ constant, for 15- and 60-ns loop propagation time.

the phase detector gain factor and the optical VCO sensitivity, respectively [see Fig. 1(b)]. $F(f)$ is the electrical loop filter transfer function defined by

$$F(f) = \frac{1}{\left(\frac{R_1}{Z_0}\left(1 + j2\pi f \tau_A\right) + \frac{j2\pi f \tau_1}{1 + j2\pi f \tau_2}\right)} \tag{3}$$

where the loop filter parameters τ_1 and τ_2 are the time constant $\tau_1 = R_1 C$ and $\tau_2 = R_2 C$, $Z_0 = 400$ kΩ and $\tau_A = 0.8$ μs are the open-loop transimpedance gain characteristics of the current feedback operational amplifier employed for the realization of the loop filter board. Usually the theoretical analysis is performed considering an ideal operational amplifier; thus, the loop natural frequency f_n and the damping factor ζ, which are conventionally used in the PLL theory, are computed as

$$f_n = \frac{1}{2\pi}\sqrt{\frac{K_{\mathrm{DC}}}{\tau_1}}, \quad \zeta = \pi f_n \tau_2. \tag{4}$$

In the OPLL design, the common way to operate is to fix the damping factor $\zeta = 1/\sqrt{2}$ and then evaluate the optimum f_n that minimizes the phase-error variance. This way, the relation between τ_1 and τ_2 is

$$\frac{\tau_2}{\sqrt{\tau_1}} = \frac{2 \cdot \zeta}{\sqrt{K_{\mathrm{DC}}}} = \text{constant}. \tag{5}$$

We discovered that this assumption is not the optimum, especially with large loop propagation delays. So, a complete analysis of the OPLL phase-error variance function, versus the loop filter parameters τ_1 and τ_2 is required.

Then, (1) was numerically integrated in order to evaluate the OPLL performance with respect to loop filter parameters. Fig. 3 shows a representation of phase-error standard deviation σ_{TOT} versus the variables τ_1 and τ_2, where the level curves are obtained by slicing the surface of σ_{TOT} with flat planes at values 5, 6, 8, and 10 degrees. The frequency noise spectrum considered in the computations includes white, flicker, and random walk contributions. The phase noise PSD $S_{\mathrm{PN}}(f)$ is defined as

$$S_{\mathrm{PN}}(f) = \frac{k_w}{f^2} + \frac{k_f}{|f|^3} + \frac{k_r}{f^4} \tag{6}$$

where k_w, k_f, and k_r are coefficients of the white frequency noise, the flicker frequency noise, and the random walk frequency noise, respectively. k_w is given by

$$k_w = \frac{\delta\nu}{\pi} \tag{7}$$

where $\delta\nu$ is the average Lorentzian spectral linewidth of the two lasers [laser A and laser B of Fig. 1(a)]. In the σ_{TOT} evaluation, the optical source phase-noise PSD coefficients assumed the following values: linewidth $\delta\nu = 10$ kHz, $k_f = 10^5$ Hz^2, and $k_r = 10^{12}$ Hz^3. Such values are typical for semiconductor lasers [17] and they performed a good comparison between theoretical and experimental data. The loop propagation delay $\tau = 15$ ns was experimentally measured. The total gain K_{DC} is 36.2 MHz. The considered $S_{\mathrm{AN}}(f)$ amplitude noise is a white Gaussian noise and its PSD is $9 \cdot 10^{-16}\mathrm{V}^2/\mathrm{Hz}$.

In Fig. 3 is shown that the minimum σ_{TOT} values are placed along a line that satisfies the condition

$$\frac{\tau_2}{\tau_1} = \frac{\text{constant}'}{K_{\mathrm{DC}}} = \text{constant} \tag{8}$$

which is in contrast with the commonly imposed condition of (5), represented by the dashed-dotted line of Fig. 3. Furthermore, Fig. 3 shows how an OPLL can optimally work on a wide range of time constants τ_1 and τ_2 values. If we consider, for example, the area delimited by the 5° level curve, the use of a higher damping factor, as suggested by Norimatsu [18], causes the dashed-dotted line of Fig. 3 to shift right in a region where the OPLL can properly work in a larger interval. As a first consequence, the OPLL would be more tolerant to components deviations from their typical values.

Fig. 4 shows the phase error standard deviation versus τ_2 when either damping factor or ratio τ_2/τ_1 set to a constant for loop delay τ equal to 15 and 60 ns. The big difference between the two conditions is quite evident especially when the loop delay is large: with $\tau = 60$ ns, fixing the ratio τ_2/τ_1 the minimum phase error standard deviation is at least 2 degrees lower with respect to working with a constant damping factor. It is clear that working with time constants ratio is preferable than fixing a damping factor value. Even if working at very low τ_2

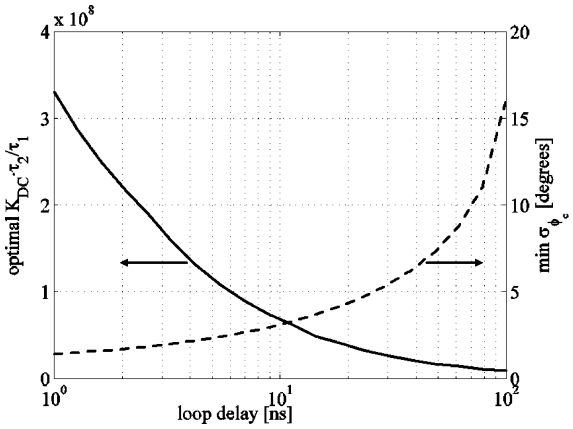

Fig. 5. Optimal $K_{\rm DC} \cdot \tau 2/\tau 1$ and minimum phase-error standard deviation against loop delay.

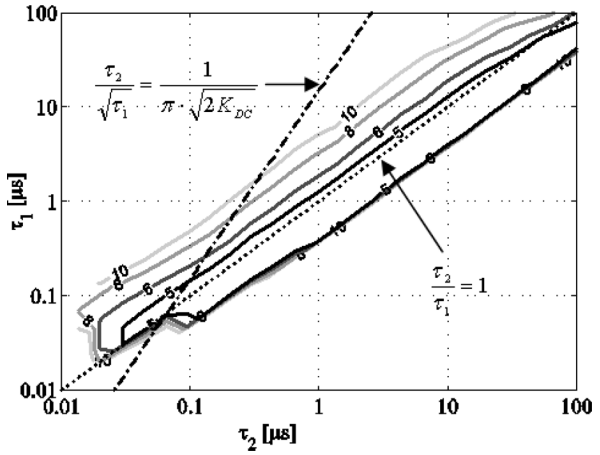

Fig. 6. Level curves of the phase error standard deviation $\sigma_{\rm TOT}$ (expressed in degrees) function of τ_1 and τ_2, obtained by experimental data post processing.

values can affect the hold-in limit and the pull-in limit, it is experimentally shown in Section II-C that an OPLL can appropriately work for τ_2 as low as 10^{-4} s.

The optimal ratio τ_2/τ_1 depends on the open loop total gain $K_{\rm DC}$ and the loop delay. Fig. 5 shows the computed relation between the loop delay and the optimal $K_{\rm DC}\,\tau_2/\tau_1$; the minimum phase-error standard deviation versus the delay is also plotted in Fig. 5.

C. Experimental Characterization

An experiment was carried out on the OPLL of Fig. 1(a) in order to confirm previous theoretical results. The experimental setup included two external cavity tunable lasers, whose measured linewidth is 10 kHz [19]. The signal power at the photo-diode input was set to -16 dBm, while the overall LO power was -3 dBm. In order to reduce the electrical noise generated by amplification circuits inside the photo-receiver, a 100-MHz electrical filter was placed at the output of the photo-diode of Fig. 1(a). The loop filter was realized with a capacitors array and a couple of trimmers in order to accurately adjust the time constants τ_1 and τ_2. The phase-error standard deviation $\sigma_{\rm TOT}$ was measured following the technique proposed in [7], where $\sigma_{\rm TOT}$ is given by

$$\sigma_{\rm TOT} = \frac{V_{\rm rms}}{K_d} \tag{9}$$

where $V_{\rm rms}$ is the rms voltage measured at the SC-OPLL photo-diode output. Experimental and simulation results were obtained evaluating the variance of the random process on an observation period equal to 10 s.

Fig. 6 shows the measured $\sigma_{\rm TOT}$ versus the time constants τ_1 and τ_2. The level curves were plotted by post-processing of the acquired experimental data. Indeed $\sigma_{\rm TOT}$ were experimentally evaluated on parallel lines of the (τ_1, τ_2) plane where the ratio τ_2/τ_1 was kept constant. For each line $\sigma_{\rm TOT}$ was measured on 24 points logarithmically spaced. The resulting measured surface of Fig. 6 matches very well the analytical one of Fig. 3. In particular, for both cases the optimum values of τ_1 and τ_2 are the ones where their ratio is constant, and both present its minimum for τ_2/τ_1 approximately equal to 1. By fixing the value of τ_2, the phase-error standard deviation $\sigma_{\rm TOT}$ becomes a function of the unique variable τ_1 and it has a bell-like shape. Furthermore, by

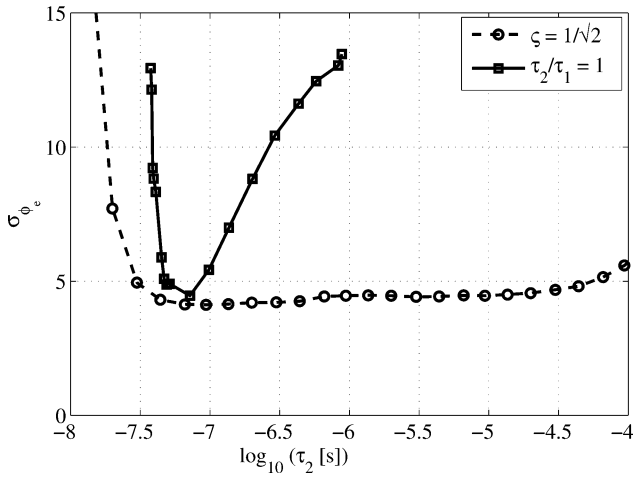

Fig. 7. Measured phase-error standard deviation versus τ_2 for the two conditions damping factor $\zeta = 1/\sqrt{2}$ and $\tau_2/\tau_1 = 1$.

increasing τ_1, the overall phase noise affects the phase-locking performance, and $\sigma_{\rm TOT}$ rises. A decrease of τ_1 results in a very rapid increase of $\sigma_{\rm TOT}$ due to the amplitude noise and the loop propagation delay. For small values of both τ_1 and τ_2 the stability of the OPLL is not guaranteed any longer, and for this reason it does not work properly.

Fig. 7 shows the measured phase-error standard deviation against τ_2 when either damping factor or ratio τ_2/τ_1 are set to a constant value. The curves match very well the analytical results of Fig. 4 thus confirming the considerations previously discussed. Furthermore, such results have the main consequence of simplifying the OPLL design procedure. It would be sufficient to fix the value of τ_2 and adjust τ_1 in order to reach the optimum value of the time constants ratio τ_2/τ_1. It is worth noting that such optimum ratio depends on the OPLL total gain $K_{\rm DC}$. A variation of the phase detector gain K_d causes a change in the optimum τ_2/τ_1. For this reason, in the following, some experiments are performed at different τ_2/τ_1 values.

A further SC-OPLL characterization was carried out in order to evaluate the PLL frequency response. This way, we wanted to estimate the error transfer function

$$H_E(f) = 1 - H(f) \tag{10}$$

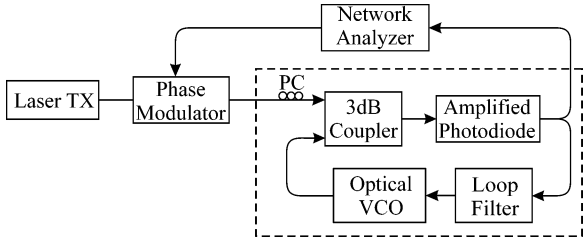

Fig. 8. Setup for measurement of the SC-OPLL error transfer function.

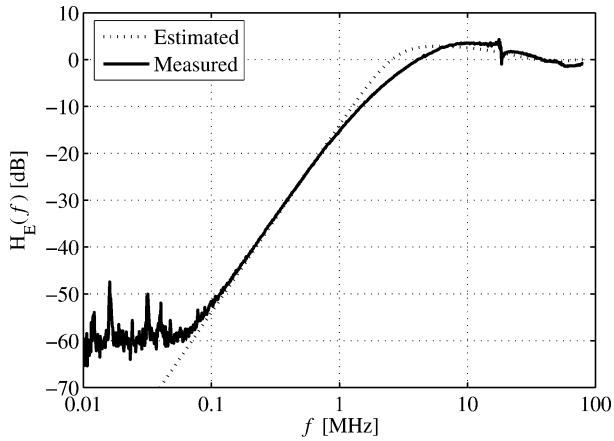

Fig. 9. Estimated and measured SC-OPLL closed-loop error transfer function.

obtained by the closed-loop OPLL transfer function defined in (2). The experimental setup is depicted in Fig. 8 as suggested in [7]. The source laser signal is phase modulated by the sweeper of the network analyzer and the frequency response is measured at the photo-diode output. The measurement was performed setting a time constant $\tau_2 = 100$ ns and $\tau_2/\tau_1 = 1$. Fig. 9 shows the error transfer function estimated by computing (10) and setting all the parameters previously defined. The corresponding response was also measured and it is also plotted in Fig. 9 which shows a good matching between theoretical and experimental results.

The SC-OPLL high pass filtering shown in Fig. 9 is characterized by a cutoff frequency higher than 4 MHz and it affects the phase of the received signal when the transmitted signal is phase modulated as explained in Section III.

III. BPSK Transmission Systems

A. Pilot Carrier SC-OPLL

Any OPLL locks the local oscillator in quadrature with respect to the received signal inhibiting optical homodyne receiver operations. In order to avoid such a problem, the transmitted signal is obtained by including a residual carrier in quadrature with respect to the phase signal $\varphi_s(t)$ proportional to the transmitted data [5], [20].

This way, the Fourier transform of the OPLL phase error $\Phi_e(f)$ is given by [7]

$$\phi_e(f) = \phi_S(f) \cdot H_E(f) \tag{11}$$

where $\Phi_S(f)$ is the Fourier transform of the phase signal. The resulting detected signal at the SC-OPLL output is proportional to the phase error through the phase detector gain K_d. Thus, the

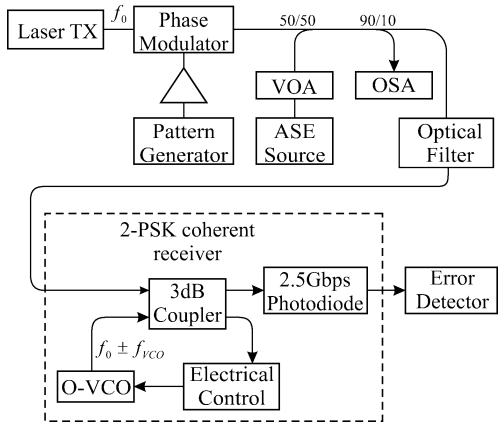

Fig. 10. Pilot carrier experimental setup with a schematic of the SC-OPLL implementation.

second-order high-pass filtering imposed by the SC-OPLL affects the phase signal. When $\varphi_s(t)$ includes a pseudo-random bit sequence (PRBS), the coherent receiver performance depends on the PRBS length. Indeed, longer PRBS includes longer sequences of the same bits 1's or 0's; for example, a $2^k - 1$ PRBS is characterized, at the most, by a k long sequence of unchanged bits. When long sequences of unchanged bits occur, the detected signal is distorted by the high-pass filtering. This behavior may also be explained by considering the spectrum of the phase signal; longer sequences have spectral components at lower frequencies that are cut by SC-OPLL high-pass filtering, inducing signal distortion.

In order to estimate the pattern dependency introduced by SC-OPLL filtering, we experimentally evaluated the system performance (see Fig. 10) for several pattern lengths. We also propose, as a solution to signal distortion, the use of 8B/10B transmission code [21], which has small spectral contents at low frequencies. Such a coding technique is also employed in ac-coupled burst-mode optical receiver applications [22]. The PSK coherent receiver is based on the SC-OPLL.

Fig. 10 shows the experimental setup. The transmitter includes an external cavity tunable laser with the same LO laser characteristics. In order to transmit a residual carrier, an NRZ signal of 3.3 $V_{\rm pp}$ was applied to the phase modulator, which requires $V\pi = 5$ V, in order to produce a 180° phase shift. Such a configuration generates a BPSK signal with a modulation angle of ±60°, by leaving a residual carrier containing 25% of the transmitted power. The amplified spontaneous emission (ASE) noise and the variable optical attenuator (VOA) add a variable amount of noise to the transmitted signal, having constant power. This configuration allows changing the optical signal-to-noise ratio (OSNR), measured by an optical spectrum analyzer (OSA) with a resolution bandwidth of 0.1 nm, and it also allows keeping the received signal power constant to −12 dBm at the coherent receiver input. The optical filter limits the noise power and it has an optical bandwidth of 0.7 nm. In order to transmit an 8B/10B encoded sequence, a $2^{22} - 1$ PRBS was encoded, and the resulting 8B/10B data were loaded into the BER tester and transmitted by its pattern generator. In order to keep a net data rate of 2.5 Gb/s, the transmitted 8B/10B coded gross data rate was increased up to 3.125 Gb/s.

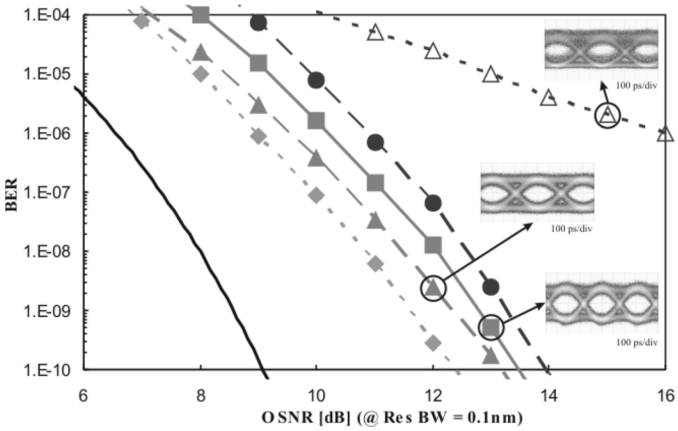

Fig. 11. Measured BER versus OSNR in 0.1-nm resolution bandwidth of 2.5-Gb/s data for different PRBS lengths (solid line: theoretical results; solid diamonds: 8B/10B encoded $2^{22}-1$; solid triangles: 2^7-1; empty triangles: 2^9-1) and 3.125 Gb/s for 8B/10B coded (solid squares: 8B/10B, encoded 2.5 Gb/s $2^{22}-1$), and decoded data (solid circles: 2.5 Gb/s $2^{22}-1$ worst case).

The homodyne receiver was based on our SC-OPLL. Since the use of a line code increases the transmitted bit rate, we used in every case an appropriate photo-diode with suitable electrical bandwidth, in order to avoid filtering penalty effects. In the SC-OPLL implementation of Fig. 1(a), in the case of 2.5-Gb/s transmission rate, we used a photo-detector with 1.8-GHz bandwidth, while for the other case of 3.125 Gb/s transmission rate we used another one with 2.3-GHz bandwidth. The loop filter was configured with $\tau_2 = 80$ ns and a $\tau_2/\tau_1 = 1.8$. A higher τ_2/τ_1 ratio was set with respect to Section II. Actually, due to the lower SC-OPLL total gain $K_{\rm DC}$ induced by the lower optical carrier power that the SC-OPLL had to lock, the new optimum ratio τ_2/τ_1 is increased.

The performance of our PSK homodyne system was evaluated through bit-error ratio (BER) measurements for various PRBS lengths. BER curves are shown in Fig. 11, where some measured eye diagrams are also presented. Initially, the pattern generator outputs 2.5 Gb/s PRBS with different lengths; Fig. 11 shows measurement results for lengths 2^7-1 and 2^9-1 with 1.8-GHz photo-diode bandwidth at the receiver. By comparing the two curves, there is an approximately 5-dB penalty at $\mathrm{BER} = 10^{-5}$ in case of 2^9-1 sequence with respect to 2^7-1. Indeed, the longer is the PRBS, the lower are the transmitted signal frequency components cut by the receiver high-pass filtering, obtaining performance degradation. Next, the 8B/10B code was employed in order to reduce the low signal frequency components. A $2^{22}-1$ PRBS was encoded and the resulting 8B/10B data were transmitted by the pattern generator at a rate of 2.5 Gb/s (coded data rate); the net data rate was 2 Gb/s. Fig. 11 shows the obtained BER curves. In this case, our system performed better than previous cases and we obtained 1-dB gain with respect to the 2^7-1 PRBS. The signal distortion due to long runs of "1's" or "0's" was extremely reduced by using the block code. Further measurements were taken at 3.125 Gb/s, so the previously used photo-diode was replaced by another one with a bandwidth of 2.3 GHz, in order to reduce the penalty introduced by incorrect electrical filtering. The encoded data were transmitted at 3.125 Gb/s corresponding to a 2.5 Gb/s net data rate. This means that the original $2^{22}-1$ PRBS is transmitted with a rate of 2.5 Gbit/s, like the cases without coding. Fig. 11 shows the measured BER against the OSNR, which presents a penalty with respect to the previous results mainly due to a larger electrical bandwidth at the receiver (the photo-diode has been changed).

Fig. 11 also shows the worst case of the BER curve for the $2^{22}-1$ PRBS after decoding. It has been calculated by assuming that a single error in the encoded bits can, at the most, generate an error burst of length 5 in the decoded domain [21]. At the end, we obtained a penalty of 1 dB with respect to the BER curve corresponding to 2.5 Gb/s 2^7-1 PRBS, demonstrating, even in the worst case, the pattern dependency suppression.

Fig. 11 presents also the theoretical BER curve, expected for the coherent receiver based on subcarrier modulation. The analysis was performed following the theory described in [23]. Since ASE noise is the only impairment that really affects our system performance, only the beat noise between LO signal and spontaneous emission was taken into account. Due to the presence of the two subcarriers at the output of OVCO, the considered beat noise has to be doubled with respect to an ideal PSK homodyne receiver, and a 3-dB penalty is taken into account. Fig. 11 compares theoretical and measured curves, showing a penalty of almost 4 dB. Such a penalty is caused for almost 3 dB by the transmission of the residual carrier; indeed, just the 75% of the transmitted power is used for data communication, while the rest of the power is related to the residual carrier that is not used for data detection. A further 1-dB penalty is due to a non-optimal polarization of the received signal and the use of a not matched electrical filter.

B. Nonlinear SC-OPLL Based on Decision-Driven Scheme

Here, we compare previous pilot carrier receiver with a nonlinear receiver still based on an SC-OPLL [13]. Such a new receiver is based on the decision-driven concept [8]. With respect to the pilot carrier SC-OPLL, it is able to detect a fully suppressed carrier transmission, so that the overall transmitted power is entirely used for data transmission. Furthermore, a decision-driven OPLL is more tolerant, with respect to the linewidth requirement, than a pilot carrier optical PLL [8]. In addition, thanks to the decision-driven block scheme, the proposed coherent optical receiver is pattern independent.

The system experimental setup is shown in Fig. 12. The transmitter is based on a LiNbO3 phase modulator, driven by an electrical NRZ 2.5 Gb/s PRBS. The optical modulated signal is a suppressed carrier 2 PSK, obtained by setting the NRZ signal amplitude equal to the phase modulator voltage $V\pi = 5$ V. Optical source, ASE noise source, VOA, and optical filter have the same specifications and functions of the previous experimental setup of Fig. 10. The adopted configuration keeps the received signal power constant to -12 dBm. Such a power is large enough to make negligible the effects of laser phase noise and electrical noise. This way, ASE noise is the only impairment that influences the performance.

The core of our experiment is the optical homodyne receiver. It is based on a modified version of the decision-driven PLL [9]. The 90° hybrid combines the two input signals in phase, at the "I" output port, and in quadrature, at the "Q" output port. It

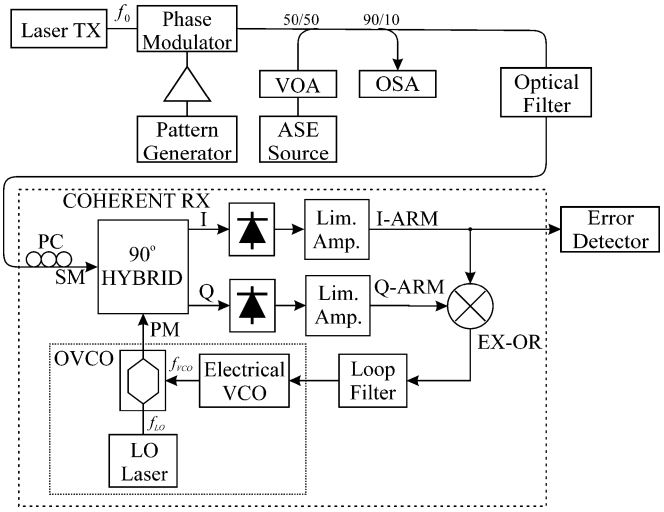

Fig. 12. Experimental setup with the coherent receiver scheme.

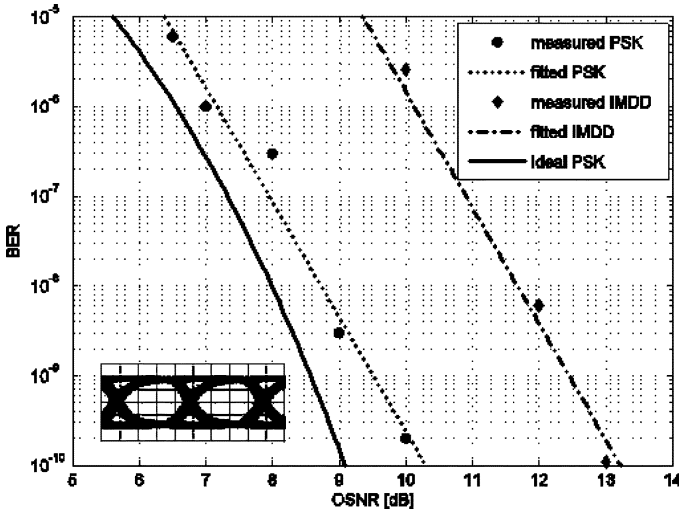

Fig. 13. Theoretical BER and measured BER versus OSNR (0.1 nm res.) of a 2.5 Gb/s BPSK transmission system (PRBS: $2^{23}-1$) and a 2.5 Gb/s IM-DD transmission system. The inset shows the eyediagram of the received signal waveforms at the output of I-ARM limiting amplifier in absence of ASE noise.

is physically a cube divided into four parts by two planar surfaces, which work, respectively, as polarizing and polarization independent beam splitters. A similar configuration was employed in [23] and a description of its operating principle is in [24]. The received light polarization state is elliptical, thanks to the use of the polarization controller PC. The light from the OVCO propagates through a polarization maintaining (PM) optical fiber, whose axis is oriented 45° with respect to the axis of the polarizing beam splitter. Two of the four 90° hybrid outputs are followed by two amplified photo-diodes, both with an overall response of 800 V/W, a bandwidth of 1.8 GHz, and a sensitivity of -24 dBm ($\mathrm{BER} = 10^{-9}$). The resulting two signal paths are called "in-phase arm" (I-ARM) and "in-quadrature arm" (Q-ARM). With respect to traditional decision-driven PLL, we employed two limiting amplifiers in both arms. The outputs of the two arms are multiplied by an "EXclusive OR" gate (EX-OR). The loop filter was configured with $\tau_2 = 80$ ns and a $\tau_2/\tau_1 = 2.6$. A higher τ_2/τ_1 ratio was set with respect to Section II. In fact, due to the lower SC-OPLL total gain K_{DC} induced by the lower optical phase detector gain K_d, the new optimum ratio τ_2/τ_1 is increased.

The LO and the source lasers were set in order to generate, respectively, two optical signals at wavelengths 1548.553 and 1548.694 nm, obtaining a 6-GHz frequency difference. The 6-GHz frequency difference guarantees a perfect locking between the subcarrier at $f_{\mathrm{LO}} - f_{\mathrm{VCO}}$ frequency and the received signal at f_{TX} frequency. The power at the 90° hybrid PM input is 4 dBm.

The PSK homodyne system performance is evaluated through BER measurements versus the received signal OSNR, and Fig. 13 shows the results. Fig. 13 presents also the same theoretical BER curve of Fig. 11, expected for the coherent receiver based on subcarrier modulation. Fig. 13 compares theoretical and measured curves and it shows a 1 dB penalty due to a non-perfect alignment of the optics in the 90° optical hybrid, a non-optimal polarization of the received signal and the use of a not matched electrical filter. A comparison of Figs. 11 and 13 reveal that SC-OPLL decision-driven based receiver performs approximately 3 dB better than the SC-OPLL pilot carrier receiver. Such an advantage is due to the ability of the decision-driven SC-OPLL in detecting a fully suppressed carrier transmission, so the overall transmitted power is entirely used for data transmission.

Fig. 13 also shows BER measurements of an equivalent intensity modulation direct detection (IM-DD) system. Such a system includes a 2.5-Gb/s IM transmitter and a DD receiver using the same amplified photo-diode and limiting amplifier included into the I-ARM of the proposed optical receiver. We use the same noise loading configuration and optical filtering employed for testing the coherent receiver. Fig. 13 compares the performance of our coherent receiver and the IM-DD transmission system. Experimental results show that the proposed coherent receiver performs 3 dB better.

IV. Conclusion

An SC-OPLL was analyzed and experimentally characterized. A novel OPLL parameters optimization procedure, useful for OPLL design operations, has been introduced. Furthermore, BPSK pilot carrier receiver experimentation has been presented and a solution for its intrinsic pattern-dependency performance, based on 8B/10B coding, has also been proposed. This simple code allows recovering the huge penalty due to the use of long PRBS. By encoding a PRBS $2^{22}-1$ and transmitting the code stream, we obtained comparable performances with respect to the transmission of a short 2^7-1 PRBS. The use of line coding shows itself as not to be necessary if a nonlinear architecture is implemented; so, a nonlinear SC-OPLL based on decision-driven scheme has been demonstrated as well. Phase locking was obtained by means of a modified version of a decision-driven PLL using subcarrier modulation. The decision was performed by simple limiting amplifiers, and the use of circuitry for clock and data recovery was proved not to be necessary in the proposed decision-driven PLL. The realized decision-driven receiver performed 3 dB better than the realized solution based on pilot carrier receiver with 8B/10B line code.

ACKNOWLEDGMENT

The authors would like to thank M. De Nichilo for his help and Avanex for its invaluable support to the experiments.

REFERENCES

[1] L. H. Enloe and J. L. Rodda, "Laser phase locked loop," *Proc. IEEE*, vol. 53, no. 2, pp. 165–166, Feb. 1965.

[2] D. J. Malyon, D. W. Smith, and R. Wyatt, "Semiconductor laser homodyne optical phase-locked-loop," *IEE Electron. Lett.*, vol. 22, no. 8, pp. 421–422, Apr. 1986.

[3] G. Fischer, "A 700 Mbit/s PSK optical homodyne system with balanced phase locked loop," *J. Opt. Commun.*, vol. 9, pp. 27–28, 1988.

[4] S. Norimatsu, H. Mawatari, Y. Yoshikuni, O. Ishida, and K. Iwashita, "10 Gbit/s optical BPSK homodyne detection experiment with solitary DFB laser diodes," *IEE Electron. Lett.*, vol. 31, pp. 125–127, 1995.

[5] L. G. Kazovsky, "Balanced phase-locked loops for optical homodyne receivers: Performance analysis, design considerations, and laser linewidth requirements," *J. Lightw. Technol.*, vol. 4, no. 2, p. 182, Feb. 1986.

[6] J. M. Kahn, "1 Gbit/s PSK homodyne transmission system using phase-locked semiconductor lasers," *IEEE Photon. Technol. Lett.*, vol. 1, no. 10, p. 340, Oct. 1989.

[7] L. G. Kazovsky and D. A. Atlas, "A 1320-nm experimental optical phase-locked loop: Performance investigation and PSK homodyne experiments at 140 Mb/s and 2 Gb/s," *J. Lightw. Technol.*, vol. 8, no. 9, p. 1414, Sep. 1990.

[8] L. G. Kazovsky, "Decision-driven phase-locked loop for optical homodyne receivers: Performance analysis and laser linewidth requirements," *J. Lightw. Technol.*, vol. 3, no. 6, p. 1238, Dec. 1985.

[9] S. Norimatsu, K. Iwashita, and K. Noguchi, "10 Gbit/s optical PSK homodyne transmission experiments using external cavity DFB LDs," *IEE Electron. Lett.*, vol. 26, pp. 648–649, 1990.

[10] H. K. Philipp, A. L. Scholtz, E. Bonek, and W. R. Leeb, "Costas loop experiments for a 10.6 μm communications receiver," *IEEE Trans. Commun.*, vol. 31, no. 8, pp. 1000–1002, Aug. 1983.

[11] T. G. Hodgkinson, "Costas loop analysis for coherent optical receivers," *Electron. Lett.*, vol. 22, p. 394, 1986.

[12] S. Camatel, V. Ferrero, R. Gaudino, and P. Poggiolini, "Optical phase-locked loop for coherent detection optical receiver," *Electron. Lett.*, vol. 40, p. 384, 2004.

[13] S. Camatel, V. Ferrero, and P. Poggiolini, "2-PSK homodyne receiver based on a decision driven architecture and a sub-carrier optical PLL," presented at the Opt. Fiber Commun. Conf. Nat. Fiber Opt. Eng. Conf., Anaheim, CA, 2006.

[14] G. L. Abbas, V. W. S. Chan, and T. K. Lee, "Local oscillator excess noise suppression for homodyne and heterodyne detection," *Opt. Lett.*, vol. 8, pp. 419–421, 1983.

[15] S. Machida and Y. Yamamoto, "Quantum-limited operation of balanced mixer homodyne and heterodyne receivers," *IEEE J. Quantum Electron.*, vol. QE-22, no. 5, p. 617, May 1986.

[16] L. G. Kazovsky, "Balanced phase-locked loops for optical homodyne receivers: Performance analysis, design considerations, and laser linewidth requirements," *J. Lightw. Technol.*, vol. LT-4, no. 2, p. 182, Feb. 1986.

[17] S. Norimatsu and O. Ishida, "Impact of flicker noise and random-walk noise on a phase-locked loop with finite propagation delay," *J. Lightw. Technol.*, vol. 12, no. 1, p. 86, Jan. 1994.

[18] S. Norimatsu and K. Iwashita, "Damping factor influence on linewidth requirements for optical PSK coherent detection systems," *J. Lightw. Technol.*, vol. 11, no. 7, p. 1226, Jul. 1993.

[19] S. Camatel and V. Ferrero, "Phase noise power spectral density measurement of narrow linewidth CW lasers using an optical phase-locked loop," *IEEE Photon. Technol. Lett.*, vol. 18, no. 23, p. 2529, Dec. 2006.

[20] T. G. Hodgkinson, "Receiver analysis for synchronous coherent optical fiber transmission systems," *J. Lightw. Technol.*, vol. LT-5, no. 4, p. 573, Apr. 1987.

[21] A. X. Widmer and P. A. Franaszek, "A DC-balanced, partitioned-block, 8B/10B transmission code," *IBM J. Res. Develop.*, vol. 27, p. 440, 1983.

[22] S. Han and M. S. Lee, "AC-coupled burst-mode optical receiver employing 8B/10B coding," *Electron. Lett.*, vol. 39, p. 1527, 2003.

[23] S. Ryu, S. Yamamoto, H. Taga, N. Edagawa, Y. Yoshida, and H. Wakabayashi, "Long-haul coherent optical fiber communication systems using optical amplifiers," *J. Lightw. Technol.*, vol. 9, no. 2, p. 251, Feb. 1991.

[24] W. R. Leeb, "Optical 90 hybrid for Costas-type receivers," *IEE Electron. Lett.*, vol. 26, pp. 1431–1432, 1990.

Stefano Camatel (M'05) received the Laurea degree in electronic engineering (*summa cum laude*) and the Ph.D. degree in electronic and communication engineering from Politecnico di Torino, Torino, Italy, in 2001 and 2005, respectively.

He is currently a Researcher with Istituto Superiore Mario Boella, Torino, Italy, where he works on free space optical communications, coherent detection, and plastic optical fiber communication systems. From June 2003 to June 2004, he was a Visiting Researcher with the University of California at Santa Barbara (UCSB), Santa Barbara. From January 2005 to December 2006, he was a Postdoctoral Researcher with Politecnico di Torino.

Valter Ferrero (M'97) received the Laurea degree (*summa cum laude*) in ingegneria elettronica from Politecnico di Torino, Torino, Italy, in 1994.

He is currently with the Optical Communication Group, Politecnico di Torino, where he supervises the PhotonLab optical laboratory conduction and directing several research projects related to optical communications. In 1994, he collaborated with Politecnico di Torino, working on optical coherent systems. From 1995 to 1996, he was with GEC Marconi, Genova, Italy. In 1997, he was in charge of the Optical Laboratory, Department of Electrical Engineering, Politecnico di Torino, and was promoted to Assistant Professor in 2001. His current research interests include optical coherent communications and free space optical communications.